https://doi.org/10.5194/egusphere-2026-3126
Preprint. Discussion started: 11 June 2026

Mineralization Mechanism and Application Potential of Vaterite Induced by Two Bacterial Strains

Xiaofang Li[1,2], Wenjun Nie[2], Zhen Guo[1], Lin Tang[2], Fuguo Liu[1], Bin Lian[2*]

[1]Shandong Provincial University Laboratory for Protected Horticulture, Shandong Facility Horticulture Bioengineering Research Center, Weifang University of Science and Technology, Weifang 262700, China

[2] College of Life Sciences, College of Marine Science and Engineering, Nanjing Normal University, Nanjing 210023, China

* Corresponding author Bin Lian, College of Life Sciences, College of Marine Science and Engineering, Nanjing Normal University, Nanjing 210023, China

Phone: +86 025 85898551 Fax: +86 025 85898551 E-mail: bin2368@vip.163.com

https://doi.org/10.5194/egusphere-2026-3126
Preprint. Discussion started: 11 June 2026

Abstract

Clarifying the bacterial mechanisms underlying vaterite biosynthesis is important for advancing biomineralization theory and expanding its applications in material science, environmental protection, and biomedicine. In this study, *Bacillus velezensis* LB002 and *Pseudomonas putida* KT2440 were used as representative bacterial strains to compare strain-dependent vaterite formation and environmental remediation performance. The biomineralization processes in the liquid medium were dynamically monitored, and the induced biominerals were characterized, with particular attention to their organic components. The differences in vaterite characteristics between both bacterial systems were evaluated, and their remediation potential was assessed using Cu^{2+} and tetracycline removal as model applications. Both strains induced vaterite formation under identical culture conditions, while *B. velezensis* exhibited a stronger biomineralization capacity than *P. putida*. In a 100 mL culture system, the Ca^{2+} mineralization percentage of *B. velezensis* reached 35.06%, and the dry weights of biomineral aggregates produced by *B. velezensis* and *P. putida* were 0.36 and 0.31 g, respectively. SEM observations revealed that the vaterite induced by *B. velezensis* had a loose and porous surface, whereas that induced by *P. putida* had a relatively smooth surface. For the high concentration of Cu^{2+} at 50 mg/L, the removal rate reached 84.93% for *B. velezensis*-induced vaterite, compared with 71.86% for *P. putida*-induced vaterite under the same conditions. Both biominerals demonstrated similar tetracycline removal performance, with removal rates of approximately 60%. These findings provide comparative evidence for strain-dependent vaterite formation and support the potential application of biogenic vaterite in environmental remediation.

Keywords: Bacteria; Biomineralization; Vaterite; Mineralization Mechanism; Cu^{2+}–TC Combined Pollution

https://doi.org/10.5194/egusphere-2026-3126
Preprint. Discussion started: 11 June 2026

1. Introduction

Microbially induced calcium carbonate precipitation (MICP) is a widespread biosedimentary process in both terrestrial and marine environments, where it contributes substantially to elemental biogeochemical cycling and the formation of marine sedimentary rocks (Dupraz et al., 2009; Diaz, et al., 2019; Wang et al., 2023). Under suitable environmental conditions, most naturally occurring microorganisms can mediate calcium carbonate synthesis (Hou et al., 2011; Li et al., 2023a; Xiao, et al., 2016; Whitaker et al., 2020). Among bacterially induced calcium carbonate biominerals, calcite, aragonite–calcite assemblages, and vaterite–calcite assemblages are the most frequently reported forms (Lyu et al., 2021; Dhami et al., 2013). The diversity of crystal polymorphs and morphologies produced during bacterial mineralization is controlled by several biological and geochemical processes. Bacterial cell walls may provide mineralization templates that promote calcium carbonate nucleation and crystal growth (Castanier et al., 2000; Li et al., 2023a). Carbonic anhydrase (CA) secreted by bacteria accelerates the hydration of CO_2 to HCO_3^-, which can subsequently be converted into CO_3^{2-} under weakly alkaline conditions and incorporated into biomineralization (Han et al., 2013; Zhang et al., 2023; Lyu et al., 2021). Extracellular polymeric substances (EPS) can regulate mineral formation because their negatively charged functional groups, including carboxyl, hydroxyl, and phosphate groups, can chelate Ca^{2+} and provide nucleation sites for biogenic calcium carbonate formation (Zhuang et al., 2018; Zhang et al., 2023). The type and abundance of organic matter generated by different bacteria during cultivation influence both the polymorph composition and structural stability of the resulting calcium carbonate biominerals (Zhu et al., 2021; Li et al., 2023a). For instance, calcite and aragonite have relatively stable crystal structures and can be formed in the presence of comparatively simple organic components (Yu et al., 2018). In contrast, vaterite is thermodynamically less stable and more difficult to induce under conventional conditions. Its initial nucleation commonly depends on amino acids or small-molecule proteins (Zhang et al., 2020; Gao et al., 2023). In most calcium carbonate mineralization systems, vaterite behaves as a metastable phase and

https://doi.org/10.5194/egusphere-2026-3126
Preprint. Discussion started: 11 June 2026

readily transforms into calcite or aragonite (Zhu et al., 2021; Li et al., 2019). However, bacterially induced vaterite has been shown to possess comparatively high structural stability. Under specific high-temperature and high-pressure conditions, it can retain its original morphology and crystal structure for extended periods without transforming into calcite or aragonite (Liu et al., 2021; Liu et al., 2023). In addition to its structural stability, *Bacillus velezensis*-induced vaterite has demonstrated strong adsorption capacities for high concentrations of heavy metals, including Cd^{2+}, Ni^{2+}, and Cu^{2+}, with maximum adsorption capacities (Q_{max}) of 172.41, 270.27, and 178.57 mg/g, respectively. These capacities are higher than those reported for conventional adsorbents such as biochar and graphene oxide (Park et al., 2016; Tan et al., 2015; Liu et al., 2019a, 2019b). Biogenic vaterite (BV) has been reported to adsorb antibiotic contaminants such as doxorubicin hydrochloride, with a Q_{max} of 447.58 mg/g (Zhang et al., 2022), suggesting that it may be applicable for the removal of typical organic pollutants. Its large specific surface area, loose porous surface structure, and favorable structural stability further support its potential use in drug loading (Li et al., 2023b) and environmental remediation (Liu et al., 2019a, 2019b; Jin et al., 2024). However, further development of BV for environmental engineering requires clarification of several issues related to biomineralization synthesis, controlling factors, and practical applicability. In particular, the key factors governing bacteria-induced BV formation, mechanisms regulating BV morphology and particle size, and feasibility of BV production by different bacterial sources as environmental remediation agents remain insufficiently defined.

Copper pollution in agricultural production systems can be derived from multiple sources. Chemical fertilizers and pesticides can introduce copper into soils, whereas certain feed additives contribute to copper accumulation in livestock breeding farms. Copper-containing compound fertilizers and organic fertilizers have particularly pronounced effects on soil copper content (Xiao et al., 2022). Long-term and excessive application of organic fertilizers, such as livestock manure, not only intensifies copper accumulation in soils but also increases antibiotic concentrations, thereby threatening soil ecological quality and human health (Wang et al., 2013; Xu, et al., 2023 Wang et al., 2021). To evaluate the potential application of BV in agricultural production, *B. velezensis* LB002 (Gram-positive, G^+) and *P. putida* KT2440 (Gram-negative, G^-) were selected as experimental strains. Both strains are typical environmental functional bacteria widely distributed in natural soils, with similar ecological niches and strong environmental adaptability. Meanwhile, they exhibit distinct inherent differences in cell wall structure, as well as the composition and secretion characteristics of extracellular polymeric substances (EPS). This controllable comparative system enables an in-depth investigation into the effects of bacterial Gram characteristics and extracellular properties on the biosynthesis, micromorphology and mineralization efficiency of vaterite. Their capacity to induce BV synthesis and the temporal characteristics of mineralization were examined under identical culture conditions. The dry weight, micromorphology, and organic composition of BV produced by the two bacterial strains were compared. The roles of fermentation broth composition, physicochemical properties, and CA activity in bacterial biomineralization were analyzed. Finally, the removal efficiencies of BV induced by the two strains for organic and inorganic pollutants were assessed. The resulting evidence provides a basis for understanding strain-dependent BV formation and evaluating the environmental application potential of biogenic vaterite.

2. Materials and Methods

2.1 Experimental Strains and Culture

B. velezensis LB002 (NCBI accession no. CP037417.1), isolated from soil, and *P. putida* KT2440 (ATCC 33015), obtained as a model strain, were used in this study. Both strains were preserved at the Key Laboratory of Microbiology and Functional Genes, Nanjing Normal University. Luria–Bertani (LB) medium was used for bacterial cultivation and mineralization induction. The medium was prepared with 1% (m/v) tryptone, 0.5% (m/v) yeast extract, and 1% (m/v) NaCl, and the initial pH was adjusted to 7.0–7.3. Bacterial cultures were incubated at 30°C and 180 rpm in a shaking incubator. Each treatment was performed with three biological replicates.

2.2 Analysis of Carbonate Mineralization Characteristics Induced by Two Bacterial Strains

Before mineralization experiments, both bacterial strains were activated in LB medium until the OD_{600} of the seed cultures reached approximately 1.2. The viable cell concentrations determined by plate counting were approximately 5×10^8 CFU/mL for *B. velezensis* and 4×10^8 CFU/mL for *P. putida*. For each mineralization treatment, 2 mL of the activated bacterial suspension was inoculated into 100 mL of LB medium supplemented with 0.8 g $CaCl_2$. This calcium concentration was selected based on the previous vaterite induction results obtained by our research group (Liu et al., 2021). An abiotic control was established using LB medium containing 0.8 g $CaCl_2$ without any bacterial inoculation. All cultures and controls were incubated at 30°C and 180 rpm for 14 d. Samples were collected after 1, 3, 5, 7, 10, and 14 d of incubation. The pH of each fermentation broth was measured using a pH meter (PHSJ-4F, Leici, China). The collected samples were centrifuged at 8000 rpm, and the supernatants were retained for Ca^{2+} analysis. The Ca^{2+} concentrations in the experimental and control groups were determined using atomic absorption spectroscopy (AA-6300C, Shimadzu, Japan). The Ca^{2+} mineralization percentage was calculated using the following equation (Li et al., 2023a).

$$\text{Percent of } Ca^{2+} \text{ mineralization } (\%) = \frac{C_{Ca^{2+}\,in\ control\ group} - C_{Ca^{2+}\,in\ experimental\ group}}{C_{Ca^{2+}\,in\ control\ group}} \times 100$$

The mixture was centrifuged at 8000 rpm for 5 min to separate the supernatant and precipitate. The precipitate was washed three times with double-distilled water, then dried in an oven at 55° C for 12 h until constant weight was achieved. The dry mass of each precipitate was measured using an analytical balance. The mineral phases of the dried products were identified using X-ray diffraction (XRD; BTX-526, Olympus, USA) with a Co target over a scanning range of 5–55°.

2.3 Comparative analysis of carbonate mineralization ability and pollutant immobilization performance induced by two bacterial strains

2.3.1 Comparison of organic composition and content of two biogenic vaterite

Preliminary tests using samples collected at different incubation stages confirmed that the calcium carbonate phase stabilized on day 7. At this stage, only slight changes in dry weight were observed, and the Ca^{2+} mineralization percentage reached an approximately steady state. Accordingly, the day-7 mineral products were selected for subsequent comparative analysis. After 7 d of incubation, the precipitates were collected, washed, and dried to a constant weight. The organic elemental compositions of the two biomineral aggregates were determined using an elemental analyzer (vario EL cube, Elementar, Germany). Fourier transform infrared spectroscopy (FTIR; Nicolet 8700, Thermo Nicolet, USA) and thermogravimetry–derivative thermogravimetry (TG-DTG; STA7300, Perkin-Elmer, USA) were used to identify the organic matter composition and quantify its content in the biominerals (Liu et al., 2019; Li et al., 2023a).

2.3.2 Comparison of Morphology of Two Biogenic Vaterite Samples

Following centrifugation and lyophilization, the biomineral powders were characterized using scanning electron microscopy coupled with energy-dispersive spectroscopy (SEM–EDS; Supra 55, Zeiss, Germany). Transmission electron microscopy (TEM; HT7700, Hitachi, Japan) was used to examine the microstructure and crystal morphology of the induced biominerals. For TEM preparation, 1.5 mL of bacterial fermentation broth was centrifuged, and the supernatant was discarded. The collected bacterial cells were fixed in 2.5% glutaraldehyde fixative for electron microscopy, embedded in epoxy resin, and sectioned into ultrathin slices using a microtome (EMUC7, Leica, Germany). The prepared sections were subsequently used for TEM observations and analyses.

2.4 Analysis of Biochemical Characteristics of Bacterial Culture Solution during Bacteria-Induced Mineralization

After 7 d of cultivation, the fermentation broths from the two bacterial strains were centrifuged, and the collected supernatants were subjected to biochemical analysis. Polysaccharide content was quantified using the phenol–sulfuric acid method, and protein content was measured using a Bradford Protein Assay Kit (Shanghai Sangon Biotech, China) (Li et al., 2023a). The ability of the fermentation supernatants to induce calcium carbonate formation was examined using a biomimetic mineralization system established according to previous methods (Lian et al., 2006; Liu et al., 2021). Excess NH_4HCO_3 was placed at the bottom of the mineralization device, and 20 mL of a mixed solution containing 0.2 mol/L $CaCl_2$ and $NaHCO_3$ was introduced into the upper layer of each group. Parallel mineralization systems were supplemented with 5 mL of fermentation supernatant from each bacterial strain or 5 mL of double-distilled water. The sealed devices were maintained at room temperature for 14 d. The minerals formed during incubation were collected and analyzed using XRD for crystal phase identification (Lian et al., 2006; Liu et al., 2021). The carbonic anhydrase (CA) activity in the bacterial supernatants was also determined to further compare the mineralization-inducing capacity of the two strains (Li et al., 2013). After centrifugation, the biomineral precipitates were dried to a constant weight, and their carbonate content was determined by acid–base titration (Li et al., 2023a).

2.5 Comparison on Removal Efficiency of Simulated Single and Combined

Pollutants by Biogenic Vaterite

Biominerals harvested after 7 d of incubation were used to evaluate the removal performance of biogenic vaterite for simulated inorganic and organic pollutants, represented by Cu^{2+} and tetracycline (TC), respectively. Single-pollutant solutions were prepared at Cu^{2+} concentrations of 10, 20, 30, 40, and 50 mg/L and TC concentrations of 5, 10, 15, 20, and 25 mg/L. Combined pollutant solutions containing both Cu^{2+} and TC were prepared using the same concentration gradients. For each treatment, 20 mL of the pollutant solution was placed in a 50 mL centrifuge tube, and 0.05 g of biogenic vaterite induced by either bacterial strain was added. The mixtures were shaken at 25°C and 120 rpm for 12 h, followed by centrifugation at 8000 rpm to separate the supernatant and precipitate. The residual Cu^{2+} concentration in the supernatant was measured using atomic absorption spectroscopy (AAS), and the residual TC content was calculated from the absorbance at 415 nm using a spectrophotometer (Rathod, et al., 2015). The adsorption-related textural properties of vaterite induced by the two bacteria were preliminarily examined through N_2 adsorption–desorption isotherm analysis using an automatic gas adsorption analyzer after degassing at 80°C for 12 h. The specific surface area was calculated using the BET model, the core theoretical model for specific surface area determination, whereas the pore size distribution was obtained using the BJH model, a classical model for 2–50 nm mesoporous pore size analysis (Wang et al., 2014; Sheng et al., 2009).

3. Results

https://doi.org/10.5194/egusphere-2026-3126
Preprint. Discussion started: 11 June 2026

3.1 Synthesis Process and Capacity Analysis of Vaterite Induced by Two Bacterial Strains

The fermentation media of the two bacterial strains were dynamically monitored to characterize vaterite formation. The pH of both fermentation broths increased gradually from day 1 to day 7 and subsequently remained at a weakly alkaline level. The pH reached approximately 8.10 for *B. velezensis* and approximately 8.30 for *P. putida* (Fig. 1a). Consistent with this pH evolution, the Ca^{2+} mineralization percentages in both bacterial systems approached equilibrium by day 7 (Fig. 1b). The measured Ca^{2+} balance indicated that only a small fraction of the consumed Ca^{2+} was directly assimilated by bacterial cells, whereas most of the consumed Ca^{2+} was immobilized in newly formed biominerals. The dry weight of the precipitates increased continuously during the first 7 d and then remained nearly constant (Fig. 1c). Based on the results shown in Fig. 1b, the Ca^{2+} mineralization percentage reached approximately 35.06% for *B. velezensis* on day 7, compared with 27.50% for *P. putida*. The corresponding dry weights of the biomineral aggregates were 0.36 and 0.31 g, respectively (Fig. 1c). Therefore, the temporal variation in precipitate dry weight was consistent with the change in the Ca^{2+} mineralization percentage (Fig. 1b and c).

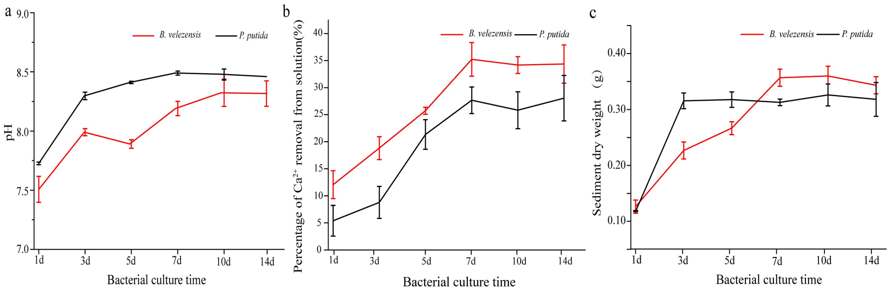

Fig. 1 Dynamic changes in key mineralization parameters induced by the two bacterial strains. (a) Variation in pH during the bacterial-induced mineralization process; (b) comparison of Ca^{2+} mineralization rates induced by the two bacterial strains; (c) comparison of the dry weights of biominerals formed by the two bacterial strains.

XRD analysis was conducted to identify the mineral phases of the biominerals induced by the two bacterial strains. No biomineral products were detected in either bacterial system on day 1. From day 3 onward, both *B. velezensis* and *P. putida* induced vaterite formation, although the vaterite diffraction peaks in the *P. putida* were relatively weak. With increasing incubation time, the crystal phase of the induced carbonate minerals remained unchanged, and vaterite was maintained as the dominant phase throughout the cultivation period (Fig. 2a and b).

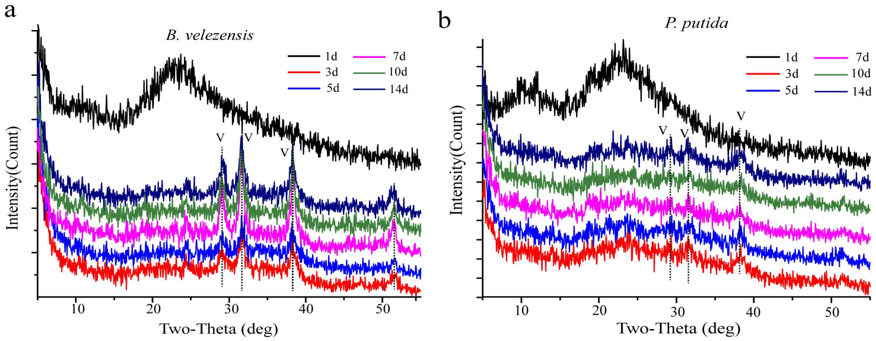

Fig. 2 XRD patterns of mineral products induced by different bacterial strains during 1–14 d of incubation.

(a) Identification of mineral products induced by *B. velezensis*; (b) identification of mineral products induced by *P. putida*.

3.2 Organic Matter Content and Mineral Characterization of Vaterite Induced by Two Bacterial Strains

Biologically induced vaterite usually contains variable amounts of organic matter (Liu et al., 2023; Li et al., 2023a; Lyu et al., 2017). In this study, the N, C, and H contents of the biomineral samples were used to evaluate the organic fraction within the mineral aggregates (Fig. 3a). The higher N and C contents suggest a higher proportion of unmineralized bacterial cells or organic constituents retained in the organic–inorganic mineral composites. This composition was accompanied by a lower relative calcium carbonate fraction and reflected weaker Ca^{2+} mineralization capacity. Elemental analysis of the day-7 biomineral aggregates indicated that the *B. velezensis*-induced vaterite contained 4.02% N, 20.89% C, and 3.27% H, whereas the *P. putida*-induced vaterite contained 6.49% N, 27.74% C, and 4.78% H. The higher elemental content measured in the *P. putida*-derived product indicated greater organic matter retention in this biomineral (Fig. 3a). In addition, FTIR characterization supported the incorporation of organic components into both biogenic vaterites. Characteristic bands assigned to -OH, -CH, and -SH were observed at 3412, 2968, and 579 cm^{-1}, respectively (Fig. 3b), confirming the presence of abundant polysaccharides and proteins. Meanwhile, typical vaterite bands were detected at 1083, 876, and 747 cm^{-1} (Liu et al., 2019). The organic matter content of the biomineral aggregates collected after 7 d of incubation was quantified using TG-DTG analysis. Because large numbers of bacterial cells were present in the precipitates, the detected organic fraction included both organic substances incorporated into the mineral matrix and residual free bacterial cells that had not been fully mineralized. The corresponding results are shown in Fig. 3c and d. The thermal mass-loss profiles of the two biominerals were divided into three stages. The first stage, occurring near 200°C, corresponded to the evaporation of bound water. The second stage, extending from 201 to 618°C, was mainly associated with the combustion of organic matter. The third stage appeared at approximately 600°C and represented biomineral decomposition, during which calcium carbonate began to decompose into CaO and CO_2. According to the mass losses recorded across these stages, the organic matter contents of the biominerals induced by *B. velezensis* and *P. putida* were calculated as 27.50% and 37.59%, respectively. The higher organic matter content in the *P.*

putida-induced biomineral aggregates (Fig. 3a) suggests a weaker mineralization capacity and greater retention of residual organic components, including bacterial cells, in the precipitates. In contrast, *B. velezensis* exhibited a stronger mineralization ability and produced precipitates with a higher calcium carbonate proportion. This pattern was consistent with the elemental analysis results (Fig. 3a).

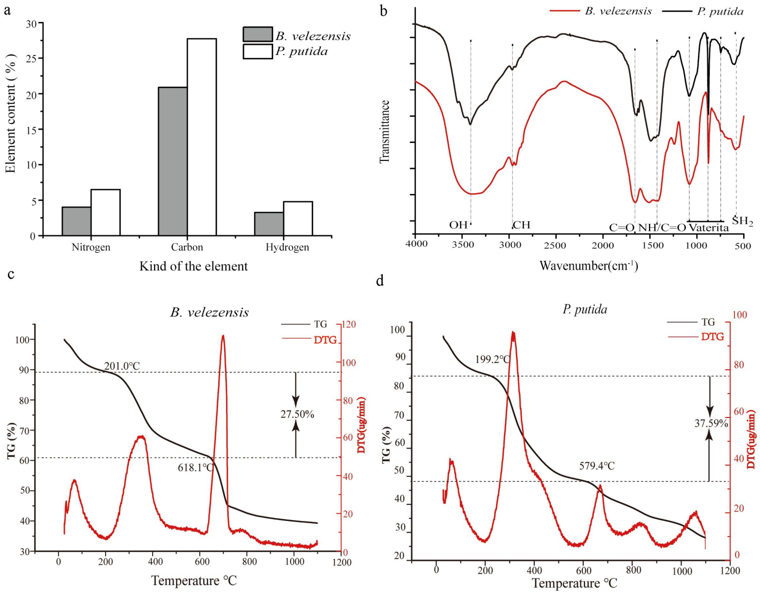

Fig. 3 Characterization of the types and contents of organic matter in biogenic vaterite. (a) Major elemental compositions of the two biomineral samples; (b) FTIR spectra of the two biomineral samples; (c) thermogravimetric analysis of biominerals induced by *B. velezensis*; (d) thermogravimetric analysis of biominerals induced by *P. putida*.

3.3 Morphological Comparison of Vaterite Induced by Two Bacterial Strains

After vaterite formation was confirmed by XRD, SEM analysis was conducted to compare the morphology of the mineral products induced by the two bacterial strains. The *B. velezensis*-induced products were composed of micro- to nanoscale vaterite particles with smaller particle sizes and a loose surface texture (Fig. 4a and b). The participation of extracellular organic matter in the mineralization process was reflected by the incorporation of bacterial cells and spores into the mineral phase, resulting in compact bacteria–mineral complexes (Fig. 4a and c). In contrast, the products induced by *P. putida* were dominated by relatively larger particles at the micron scale, and the corresponding biomineral complexes contained a higher proportion of organic matter (Fig. 4d and e). EDS analysis indicated that the *P. putida*-induced vaterite was characterized by higher carbon content and lower calcium content than the *B. velezensis*-induced vaterite (Fig. 4f). This revealed relatively lower degree of carbonate mineralization and confirmed the stronger mineralization-inducing capacity of *B. velezensis*.

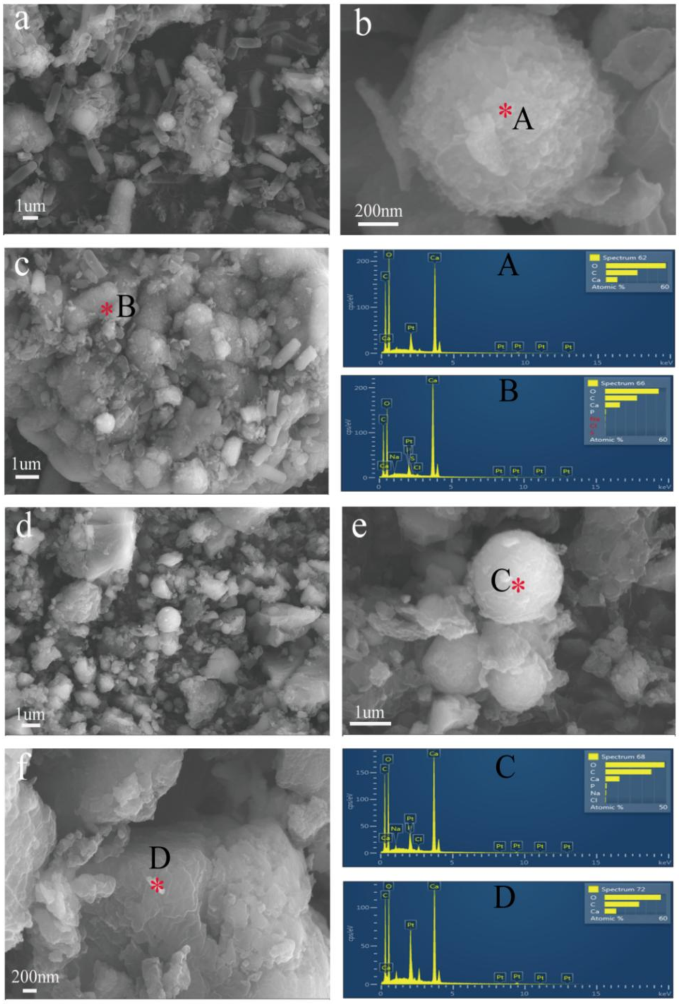

Fig. 4 SEM-EDS characterization of biogenic vaterite induced by the two bacterial strains. (a–c) Morphological characterization of biominerals induced by *B. velezensis*; (A–B) corresponding EDS spectra of the selected regions shown in panels (a–c); (d–f)

morphological characterization of biominerals induced by *P. putida*; (C–D) corresponding EDS spectra of the selected regions shown in panels (d–f).

Surface-associated mineralization of the two bacterial strains was examined using TEM. *B. velezensis* retained a rod-shaped morphology, and numerous acicular mineral particles were distributed around the bacterial cells (Fig. 5a and b). The *P. putida* cells appeared spherical, with biomineral material attached to their surface (Fig. 5c and d). However, the selected area electron diffraction (SAED) analysis of the mineralized surfaces of both bacterial strains did not reveal characteristic diffraction patterns corresponding to vaterite.

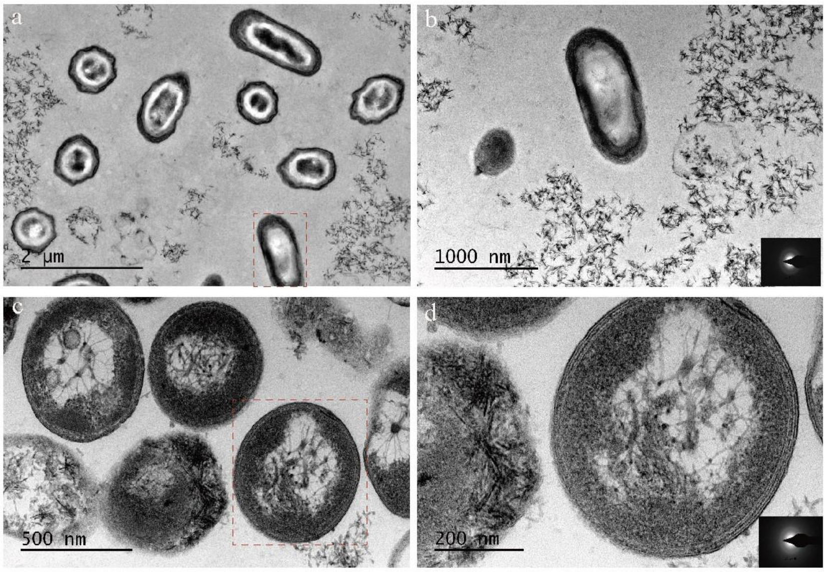

Fig. 5 TEM and SAED analyses of bacterial surface mineralization. (a) TEM observation of surface mineralization in *Bacillus velezensis*; (b) cellular morphology of *Bacillus velezensis*; (c) cellular morphology of *Pseudomonas putida*; (d) selected area electron diffraction (SAED) analysis of bacterial surface mineralization.

3.4 Analysis of Biochemical Characteristics of Culture Solution Related to Bacterial Mineralization

The carbonic anhydrase (CA) activity differed markedly between the two bacterial fermentation broths. The CA activity measured in the *B. velezensis* broth was approximately five times higher than that in the *P. putida* broth (Fig. S1a). Consistent with this difference, titration analysis demonstrated that the carbonate proportions in the biominerals induced by *B. velezensis* and *P. putida* were 38.93% and 24.26%, respectively (Fig. S1b). The biochemical compositions of the 7-day fermentation broths were analyzed. *B. velezensis* secreted a significantly higher polysaccharide content than *P. putida*, with values of 0.53 and 0.33 g/L, respectively (Fig. S1c). Conversely, the protein content in *P. putida* reached 0.024 g/L, which was higher than that of 0.014 g/L in *B. velezensis* (Fig. S1d). Subsequently, biomimetic mineralization experiments were performed using fermentation supernatants from both bacterial strains, along with dextran and bovine serum albumin. The fermentation broths of both *B. velezensis* and *P. putida* partially converted calcite to vaterite, whereas ultrapure water did not induce this phase transformation (Fig. S2). These results suggest that CA promotes the generation of carbonate ions, thereby facilitating their subsequent binding with calcium ions to form calcium carbonate. Protein components may contribute to vaterite biosynthesis and stabilization during mineralization.

3.5 Comparison of Removal Efficiency of Organic-Inorganic Pollutants by Vaterite Induced by Two Bacterial Strains

The environmental application potential of the two biogenic vaterites was assessed by comparing their removal performance for inorganic and organic pollutants. In both single- and combined-pollutant systems, *B. velezensis*-induced vaterite showed a stronger capacity for Cu^{2+} removal than *P. putida*-induced vaterite. At a high Cu^{2+} concentration of 50 mg/L, the removal efficiencies of the *B. velezensis*-induced vaterite reached 84.37% and 84.93%, respectively (Fig. 6a and b), whereas those of the *P. putida*-induced vaterite were 69.16% and 71.86% under the same conditions. The limited difference between the single and combined systems indicates that the introduction of TC exerted only a minor effect on Cu^{2+} adsorption by vaterite. At lower Cu^{2+} concentrations (10–20 mg/L), the *B. velezensis*-induced vaterite maintained higher removal efficiencies than the *P. putida*-induced vaterite. This stronger heavy metal removal performance was associated with its larger specific surface area and pore structure, with a specific surface area of 13.19 m^2/g and an average pore size of 4.88 nm, compared with 2.56 m^2/g and 4.13 nm for the *P.*

putida-induced vaterite, respectively (Table S1). In the single TC system, the *P. putida*-induced vaterite presented a higher TC removal rate at the low TC concentration of 5 mg/L, reaching 64.94% compared with 49.08% for the *B. velezensis*-induced vaterite. As the TC concentration increased, the removal efficiencies of both biominerals increased and gradually approached approximately 70% (Fig. 6c). In the combined-pollutant system, Cu^{2+} addition reduced TC removal by both types of biogenic vaterite (Fig. 6d). This reduction was mainly attributed to the preferential occupation of adsorption sites by Cu^{2+}, whereas TC, with its relatively larger molecular size, exhibited weaker competitive access to these sites. Overall, *B. velezensis*-induced vaterite exhibited more favorable removal performance, particularly for Cu^{2+} immobilization, supporting its potential application in pollutant remediation.

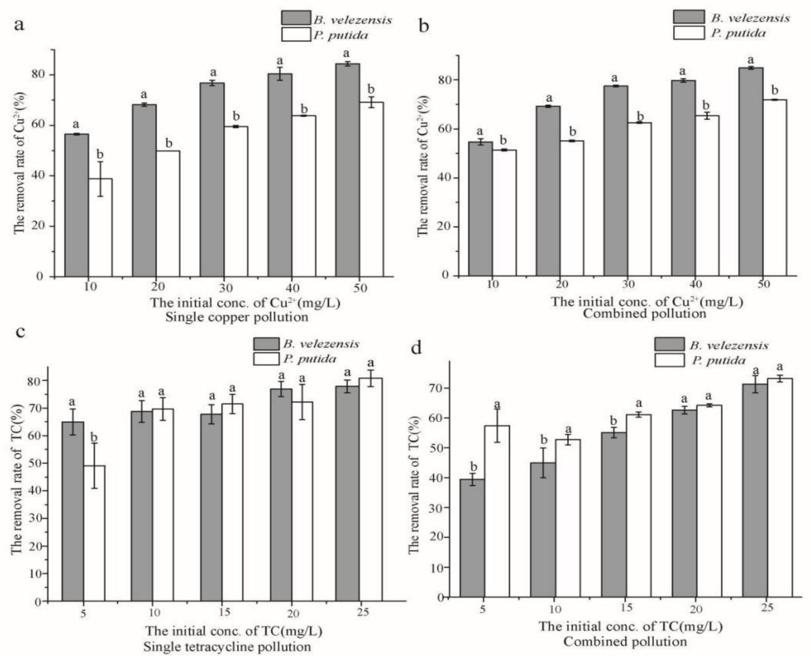

Fig. 6 Comparison of pollutant removal performance by biogenic vaterite induced by the two bacterial strains. (a) Removal efficiency of Cu^{2+} under single-pollutant conditions; (b) removal efficiency of tetracycline (TC) under single-pollutant conditions; (c) removal efficiency of Cu^{2+} under combined-pollution conditions; (d)

https://doi.org/10.5194/egusphere-2026-3126
Preprint. Discussion started: 11 June 2026

removal efficiency of TC under combined-pollution conditions.

4. Discussion

4.1 Key Controlling Factors for Bacterially Induced Vaterite Synthesis

B. velezensis is a Gram-positive (G^+) bacterium with surface flagella and the ability to form endospores. It commonly colonizes soil and plant surfaces and is widely used as a probiotic strain in agricultural production. *P. putida* is a Gram-negative ($G^–$), ovoid, lophotrichous bacterium that is broadly distributed in natural environments. Although both strains differ markedly in cell type and physiological characteristics, they are capable of inducing biogenic vaterite formation in Ca^{2+}-supplemented culture systems. During mineralization, the pH increased from day 1 to day 3 of incubation (Fig. 1a). This early alkaline shift was accompanied by the CA-mediated conversion of CO_2 into HCO_3^-, which subsequently participated in Ca^{2+} binding and calcium carbonate formation under alkaline conditions. The most rapid increase in precipitate dry weight also occurred during this period (Fig. 1c), followed by stabilization on day 7 (Fig. 1). However, the mineralization efficiency differed substantially between these two strains. The Ca^{2+} mineralization ratio reached 35.06% in the *B. velezensis* system, whereas only 27.50% was achieved in the *P. putida* (Fig. 1b). This difference indicates that *B. velezensis* provides a more favorable biological environment for biogenic vaterite formation. The stronger mineralization performance of *B. velezensis* was closely associated with differences in bacterial cell wall structure and extracellular polymeric substances (EPS). The cell wall properties and EPS composition can affect both the crystal type and micromorphology of biogenic calcium carbonate. Among EPS components, proteins are particularly important because they provide nucleation sites for vaterite formation (Zhang et al., 2021; Gao et al., 2023). Although both strains induced vaterite under identical culture conditions, their mineral products exhibited evident morphological differences. *B. velezensis*-induced vaterite exhibited a loose, porous, and layered surface structure. The polysaccharides secreted by *B. velezensis* appeared to promote the binding of vaterite particles to bacterial cells, resulting in compact bacteria–mineral complexes (Fig. 4c). In contrast, the *P. putida*-induced vaterite presented a smoother surface and lacked a layered microstructure. The lower polysaccharide content in the *P. putida* culture system weakened cell–mineral adhesion and restricted the formation of large bacteria–mineral aggregates (Fig. 4d). These observations suggest that the morphology of biogenic vaterite is largely regulated by the composition, type, and abundance of EPS in the fermentation broth. In addition to EPS composition, bacterial culture pH and CA activity were involved in regulating calcium carbonate synthesis. During vaterite formation, proteins act mainly as nucleation sites for crystal initiation, whereas polysaccharides mediate adhesion between bacterial cells and mineral particles, thereby promoting the development of bacteria–mineral aggregates. Biomimetic mineralization experiments showed that protein molecules were the dominant contributors to biogenic vaterite formation (Fig. S2), while polysaccharides primarily promoted mineral-particle adhesion and aggregate enlargement (Fig. 4b). This pattern is consistent with the findings of Zhang et al. (2020) and supports the involvement of EPS in fermentation broth-mediated biomineralization. Given the high compositional complexity of bacterial fermentation broth, components other than polysaccharides and proteins, such as organic acids, may participate in regulating the formation of different calcium carbonate polymorphs. Therefore, further studies are needed to clarify how the content and composition of polysaccharides and proteins modulate calcium carbonate morphology and bacteria–mineral complex formation.

Taken together, vaterite synthesis induced by the two bacterial strains was governed by the combined effects of bacterial cell wall properties, extracellular metabolites, and mineralization conditions (Fig. 7). Both strains were able to induce biogenic vaterite under suitable culture conditions, and the mineralization process was closely related to pH variation and CA activity. Nevertheless, *B. velezensis* presented a stronger mineralization tendency and higher mineralization capacity. Extracellular metabolites, particularly proteins and polysaccharides, are key regulators of extracellular bacterial mineralization. Proteins promoted vaterite nucleation and formation, whereas polysaccharides strengthened biomineral particle adhesion and supported the development of larger bacteria–mineral complexes. Consequently, although both strains produced biogenic vaterite, the resulting minerals differed markedly in terms of surface microstructure and pollutant immobilization performance. The higher Ca^{2+} mineralization rate and larger specific surface area of *B. velezensis*-induced vaterite indicate that this biomineral has greater potential for practical application.

4.2 Synthesis Mode of Biogenic Vaterite

Compared with chemically synthesized vaterite, bacterially induced biogenic vaterite generally exhibits more complex morphology and higher structural stability, making it less prone to transformation into aragonite or calcite (Liu et al., 2021). This difference is mainly associated with the involvement of abundant organic matter, especially protein components, which can function as nucleation sites during vaterite formation. Both *B. velezensis* and *P. putida* secreted substantial EPS, including polysaccharides and proteins. However, the higher CA activity of *B. velezensis* promoted greater Ca^{2+} precipitation as calcium carbonate in the culture system. In addition, the dense peptidoglycan layer in the *B. velezensis* cell wall could provide a mineralization template, whereas the carboxyl and phosphate groups in teichoic acid could bind environmental metal cations and immobilize more Ca^{2+} in the culture system (Zhang et al., 2021; Li et al., 2023a). These findings suggest that Gram-positive bacteria have a stronger cell-wall-mediated mineralization capacity and are more likely to form bacteria–mineral complexes through the combined effects of cell walls and extracellular polysaccharides (Fig. 7). The weaker mineralization performance of *P. putida* was supported by organic matter and carbonate analyses. TG-DTG results showed that P. putida-induced biogenic vaterite contained a higher organic matter content, indicating that its bacteria–mineral aggregates retained more unmineralized bacterial cells or organic components. This higher organic fraction corresponded to a lower mineralization-inducing capacity in the *P. putida* system. Quantitative carbonate titration showed that the carbonate content of *P. putida*-induced vaterite was approximately 14.7% lower than that of *B. velezensis*-induced vaterite, confirming that organic components accounted for a larger proportion of the former mineral structure (Figs. 2a and S1b). Biogenic vaterite induced by the two bacterial strains has been explored to show the potential for heavy metal and organic pollutant treatment. For Cu^{2+} pollution, *B. velezensis*-induced biogenic vaterite had micro- to nanoscale particles and a large specific surface area, which contribute to its effective removal of heavy metal ions (Liu et al., 2019). In contrast, the *P. putida*-induced vaterite had a smaller specific surface area and weaker Cu^{2+} adsorption performance. For TC pollution, the removal efficiencies of biogenic vaterite induced by *B. velezensis* and *P. putida* differed only slightly, and both materials effectively reduced the TC concentration (Fig. 6a and b). The large surface pore size and specific surface area of bacterially induced biogenic vaterite support its potential application in pollutant remediation. However, the differences in bacterial sources produced significant variations in mineral morphology and surface structure, which affected pollutant adsorption performance. Therefore, *B. velezensis*-induced biogenic vaterite is more competitive for applications such as agricultural soil improvement. The proposed model by which the two bacteria induced calcium carbonate mineralization and retained combined pollutants is shown in Fig. 7.

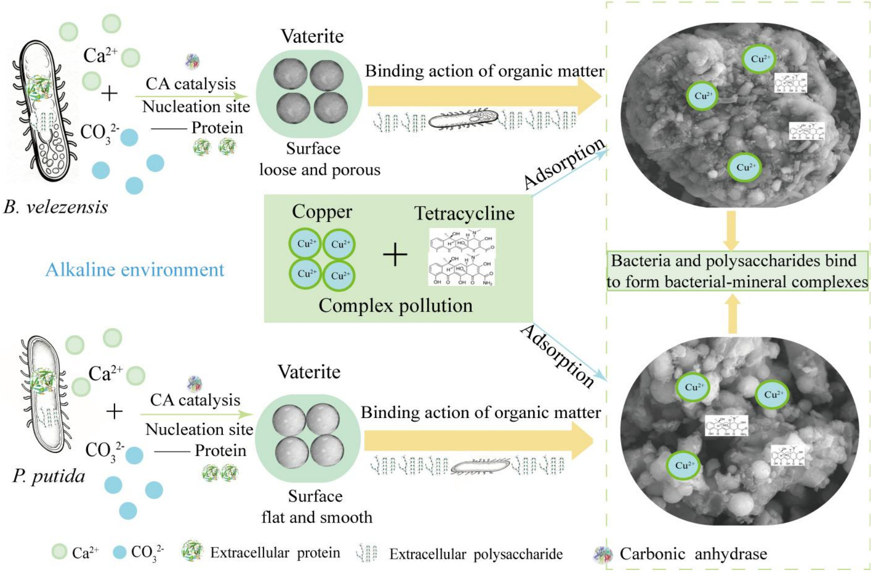

Fig. 7 Proposed schematic model of calcium carbonate mineralization and combined pollutant immobilization induced by the two bacterial strains.

4.3 Environmental Application Potential of Biogenic Vaterite

Compared with chemically synthesized vaterite, which is prone to phase transformation into aragonite and calcite, bacterially induced biogenic vaterite has a more stable structure and can sustain long-term adsorption capacity. This stability is mainly associated with the participation of organic matter, particularly proteins, in nucleation (Liu et al., 2023; Sarkar et al., 2010; Wang et al., 2009). The specific surface area of *B. velezensis*-induced vaterite reached 13.19 m^2/g, which was substantially higher than that of *P. putida*-derived vaterite (2.56 m^2/g). The loose and porous structure of *B. velezensis*-induced vaterite provided abundant adsorption sites and enabled a removal rate of 84.93% for high concentrations of Cu^{2+} at 50 mg/L. This removal performance was higher than that reported for several conventional adsorbents, including biochar and graphene oxide (Park et al., 2016; Tan et al., 2015).

Biogenic vaterite is derived from microbial metabolism and is expected to exhibit favorable potential compatibility with environmental matrices, such as soil and water. Unlike chemically synthesized materials, its production does not introduce residual toxic additives from the synthesis process. Because it is composed mainly of calcium carbonate and natural organic matter, biogenic vaterite has the potential to undergo natural degradation or transformation in the environment with a low risk of secondary pollution. In the Cu^{2+}–TC combined pollution system, the *B. velezensis*-induced vaterite maintained a Cu^{2+} removal rate above 84%, whereas TC removal decreased slightly because of competitive adsorption. This dual-removal behavior is important because conventional single-function adsorbents often have limited ability to treat inorganic and organic contaminants simultaneously, thereby expanding the potential application scenarios of biogenic vaterite (Fig. 6d). However, its practical implementation is still restricted by high cultivation costs and low production efficiency. The LB medium used in this study was costly, and the medium-related raw material costs would represent a major proportion of the total expenses during scale-up. In addition, *B. velezensis*-induced mineralization required 7 d to reach Ca^{2+} mineralization equilibrium, and only 0.36 g of biogenic vaterite was obtained from a 100 mL culture system (Fig. 1c). This low yield limits its direct utilization for large-scale pollution remediation. To reduce production costs, future studies should explore the substitution of LB medium with agricultural waste, such as straw hydrolysate and livestock manure fermentation broth (Li et al., 2023c). For practical applications, biogenic vaterite may be prioritized for small-scale, high-concentration, and high-risk pollution scenarios, including heavy metal–antibiotic co-contaminated soils around livestock farms and industrial wastewater pretreatment. Its combination with existing remediation technologies, such as soil leaching and biological composting, may further improve overall remediation efficiency through functional complementation.

5. Conclusion

This study compared the characteristics, formation mechanisms, and simulated environmental applications of vaterite induced by *B. velezensis* and *P. putida* under identical culture conditions. As a Gram-positive strain, *B. velezensis* showed a stronger calcium carbonate mineralization capacity than the Gram-negative strain *P. putida*, with carbonate mineralization percentages of 35.06% and 27.50%, respectively. The mineralization capacity was mainly associated with EPS composition and carbonic anhydrase activity, whereas the crystal type of bacterially induced calcium carbonate was regulated by extracellular proteins. The *B. velezensis*-induced vaterite developed a loose and porous surface structure with a relatively large specific surface area. The removal rates for high-concentration Cu^{2+} and TC reached 84.37% and 80.81%, respectively, indicating its potential applicability in the remediation of heavy metal and organic pollutant contamination.

Data availability.

All datasets obtained for this study are included in the manuscript/Supplementary Material.

Author contributions.

Xiaofang Li: Conceptualization, Methodology, Formal analysis, Writing original draft – review & editing, Funding acquisition. Wenjun Nie: Conceptualization, Methodology, Validation. Zhen Guo: Formal analysis, Investigation. Lin Tang: Methodology, Formal analysis. Fuguo Liu: Formal analysis, Investigation. Bin Lian: Methodology, Formal analysis, Writing – review & editing

Competing interests.

The contact author has declared that none of the authors has any competing interests.

Acknowledgements.

This work was supported by the the Natural Science Foundation of Shandong Province (No. ZR2025QC384) and the Doctoral Fund of Weifang University of Science and Technology (No. KJRC2023048).

References

Castanier, S., Métayer-Levrel, G.L., and Perthuisot, J.P.: Bacterial roles in the precipitation of carbonate minerals. Springer Berlin Heidelberg. 2000

Diaz, M.R., and Eberli, G. P.: Decoding the mechanism of formation in marine ooids: A review, Earth-Science Reviews., 190, 536-556, https://doi.org/10.1016/j.earscirev.2018.12.016, 2019.

Dhami, N.K., Reddy, M.S., and Mukherjee, A.: Biomineralization of calcium carbonates and their engineered applications: a review. Front. Microbiol., 4. https://doi.org/10.3389/fmicb.2013.00314, 2013.

Dupraz, C., Reid, R.P., Braissant, O., Decho, A.W., Norman, R.S., and Visscher, P.T.: Processes of carbonate precipitation in modern microbial mats. Earth-Sci. Rev., 96(3), 141-162. https://doi.org/10.1016/j.earscirev.2008.10.005, 2009.

Gao, X., Li, J., Hu, K., Zhao, Y., Han, Y., Liu, F., Tucker, M.E., and Han, Z.Z.: Calcification of cell membranes: From ions to minerals. Chem. Geol., 617, 121266, https://doi.org/10.1016/j.chemgeo.2022.121266, 2023.

Han, J., Lian, B., and Ling, H.: Induction of calcium carbonate by *Bacillus cereus*. Geomicrobiol. J., 30(8), 682-689, 10.1080/01490451.2012.758194, 2013.

Hou, W., Lian, B., and Zhang X.: CO_2 mineralization induced by fungal nitrate assimilation. Bioresource Technol., 102, 1562-1566, 10.1016/j.biortech.2010.08.080, 2011.

Jin, B., Wang, S., Lei, Y., Jia, H., Niu, Q., Dapaah, M., Gao, Y., and Cheng, L.: Green and effective remediation of heavy metals contaminated water using $CaCO_3$ vaterite synthesized through biomineralization. J. Environ. Manage., 353, 120136, https://doi.org/10.1016/j.jenvman.2024.120136, 2024,

Lian, B., Hu, Q., Chen, J., Ji, J., and Teng, H.:Carbonate biomineralization induced by soil bacterium *Bacillus megaterium*. Geochim. Cosmochim. Ac., 70(22), 5522-5535. 10.1016/j.gca.2006.08.044, 2006.

Li, H., Yao, Q., Wang, F., Huang, Y., Fu, S., and Zhou, G.: Insights into the formation mechanism of vaterite mediated by a deep-sea bacterium *Shewanella piezotolerans* WP3. Geochim. Cosmochim. Ac., 256, 35-48, 10.1016/j.gca.2018.06.011, 2019.

Li, X., He, X., Ren, K., Dong, H., and Lian B.: Mechanisms of carbonate precipitation induced by two model bacteria. Chem. Geol. 628, 121461, https://doi.org/10.1016/j.chemgeo.2023.121461, 2023a.

Li, S., and Lian, B.: Application of calcium carbonate as a controlled release carrier for therapeutic drugs. Minerals-Basel, 13(9), 1136, https://doi.org/10.3390/min13091136, 2023b.

Li, J., Feng, Y., Qiu, Y., Chen, D., Liang, D., Zhou, J., and Liu, G.: Recovery of electron and carbon source from agricultural waste corncob by microbial electrochemical system to enhance wastewater denitrification. Sci. Total Environ., 878, 162926, https://doi.org/10.1016/j.scitotenv.2023.162926, 2023c.

Lyu, J., Ma, F., Li, F., Zhang, C., and Chen, J.: Vaterite induced by *Lysinibacillus* sp. GW-2 strain and its stability. J. Struct. Biol., 200 (2), 97-105, 10.1016/j.jsb.2017.09.008, 2017.

Lyu, J., Li, F., Zhang, C., Gower, L., Wasman, S., Sun, J., Yang, G., Chen, J., Gu, L., Tang, X., and Scheiffele, G. From the inside out: Elemental compositions and mineral phases provide insights into bacterial calcification. Chem. Geol., 559, 119974, https://doi.org/10.1016/j.chemgeo.2020.119974, 2021.

Liu, R., Huang, S., Zhang, X., Song, Y., He, G., Wang, Z., and Lian, B.: Bio-mineralisation, characterization, and stability of calcium carbonate containing organic matter. Rsc Adv., 11(24), 14415-14425, https://doi.org/10.1039/D1RA00615K, 2021.

Liu, R., and Lian, B. Immobilisation of Cd(II) on biogenic and abiotic calcium carbonate. J. Hazard. Mater., 378, 120707-120718, https://doi.org/10.1016/j.jhazmat.2019.05.100, 2019a.

Liu, R., and Lian, B.: Non-competitive and competitive adsorption of Cd^{2+}, Ni^{2+}, and Cu^{2+} by biogenic vaterite. Sci. Total Environ., 659, 122-130, https://doi.org/10.1016/j.scitotenv.2018.12.199, 2019b.

Liu, H., Huang H., Nie W., Sun M., Li, X., and Lian, B.: Facilitated mechanism of biological vaterite stability mediated by *Bacillus velezensis* and its secretions. ACS Earth Space Chem., 7(10), 2019-2030. https://doi.org/10.1021/acsearthspacechem.3c00135, 2023.

Park, J.H., Ok, Y.S., Kim, S.H., Cho, J.S., Heo, J.S., Delaune, R.D., and Seo, D.C.: Competitive adsorption of heavy metals onto sesame straw biochar in aqueous solutions. Chemosphere, 142, 77-83, https://doi.org/10.1016/j.chemosphere.2015.05.093, 2016.

Rathod, M., Haldar, S., and Basha, S.: Nanocrystalline cellulose for removal of tetracycline hydrochloride from water via biosorption: Equilibrium, kinetic and thermodynamic studies. Ecological Engneering, 84, 240-249, https://doi.org/10.1016/j.ecoleng.2015.09.031, 2015

Sarkar, A., and Mahapatra, S.: Synthesis of all crystalline phases of anhydrous calcium carbonate. Cryst. Growth Des., 10 (5), 2129-2135, https://doi.org/10.1021/cg9012813, 2010.

Sheng, G., Wang, S., Hu, J., Lu, Y., Li, J., Dong, Y., and Wang, X.: Adsorption of Pb(II) on diatomite as affected via aqueous solution chemistry and temperature. Colloids Surfaces A, 339(1), 159-166, 10.1016/j.colsurfa.2009.02.016, 2009.

Tan, P., Sun, J., and Hu, Y.: Adsorption of Cu^{2+}, Cd^{2+} and Ni^{2+} from aqueous single metal solutions on graphene oxide membranes. J. Hazard. Mater., 297, 251-260, https://doi.org/10.1016/j.jhazmat.2015.04.068, 2015.

Wang, X., Kong, R., Pan, X., Xu, H., Xia, D., Shan, H., Lu, J.: Role of Ovalbumin in the stabilization of metastable vaterite in calcium carbonate biomineralization. J. Phys. Chem. B, 113 (26), 8975-8982, https://doi.org/10.1021/jp810281f, 2009.

Wang X., Yang L., Zhang J., Wang, C., and Li, Q.: Preparation and characterization of chitosan – poly(vinyl alcohol)/bentonite nanocomposites for adsorption of Hg(II) ions. Chem. Eng. J., 251(9), 404-412, 10.1016/j.cej.2014.04.089, 2014.

Wang, Y., Konstantinou, C., Tang, S., and Chen, H., Applications of microbial-induced carbonate precipitation: A state-of-the-art review. Biogeotechnics, 1(1), 100008. https://doi.org/10.1016/j.bgtech.2023.100008, 2023.

Wang, H., Dong, Y., Yang Y, Toor, G.S., and Zhang, X.M.: Changes in heavy metal contents in animal feeds and manures in an intensive animal production region of China. J. Environ. Sci., 25(12), 2435-2442. 10.1016/S1001-0742(13)60473-8, 2013.

Wang, X., Yan, X., and Li, X.: Environmental safety risk for application of anaerobic fermentation biogas slurry from livestock manure in agricultural land in China. Scientia Agricultura Sinica, 54 (1) , 110-139, 2021.

Whitaker, J.M., Vanapalli, S., and Fortin, D.: Improving the strength of sandy soils via ureolytic $CaCO_3$ solidification by *Sporosarcina ureae*. Biogeosciences, 15 (14), 4367-4380, https://doi.org/10.5194/bg-15-4367-2018, 2018.

Xiao, L., and Lian, B.: Heterologously expressed carbonic anhydrase from *Bacillus mucilaginosus* promoting $CaCO_3$ formation by capturing atmospheric CO_2. Carbonates and Evaporites, 31(1), 39-45. 10.1007/s13146-015-0239-4, 2016.

Xiao, M., Xu, S., Yang, B., Zeng, G., Qian, L., Huang, H., and Ren, S. L.: Contamination, source apportionment, and health risk assessment of heavy metals in farmland soils surrounding a typical copper tailings pond. Int. J. Env. Res. Pub. He., 19, 14264, https://doi.org/10.3390/ijerph192114264, 2022.

Xu, Y., Zhu, L., Chen, S., Li, R., Li, J., Yuan, J., Wen, T., Xue, C.,and Shen, Q.: Risk assessment and dissemination mechanism of antibiotic resistance genes in compost. Environ. Int., 178, 108126, 10.1016/j.envint.2023.108126, 2023.

Yu, L., Li, Q., Chen C., Lu Z., and Wang X.: The effects of two kinds of extracellular monosaccharides on the mineralization of calcium carbonate. Acta Petrologica et Mineralogica, 37(3), 497-504, 2018.

Zhang, C., Li, X., Lyu, J., and Li, F.: Comparison of carbonate precipitation induced by *Curvibacter* sp. HJ-1 and *Arthrobacter* sp. MF-2: Further insight into the biomineralization process. Journal of Structural Biology, 212(2), 107609, 10.1016/j.jsb.2020.107609, 2020.

Zhang, C., Li, F., Lyu, J., and Yao, Y.: Biomimetic mineralization of Ca-Mg carbonates: relevance to microbial cells and extracellular polymeric substances, Microsc. Microanal., 29, (2), 665-674 https://doi.org/10.1093/micmic/ozac044, 2023.

Zhang, L., Sun, P., An, X., Wang, X., Li, S., and Lian, B., Vaterite synthesized by waste liquid of extracting chitin from crab shells and the mineral loading for doxorubicin hydrochloride. Minerals-Basel, 12(12), 1608 https://doi.org/10.3390/min12121608, 2022.

Zhuang, D., Yan, H., Tucker, M., Zhao, H., Han, Z., Zhao, Y., Sun, B., Li, D., Pan, J., Zhao, Y., Meng, R., Shan, G., Zhang, X.,and Tang, R.: Calcite precipitation induced by *Bacillus cereus* MRR2 cultured at different Ca^{2+} concentrations: Further insights into biotic and abiotic calcite. Chem. Geol., 500, 64-87, https://doi.org/10.1016/j.chemgeo.2018.09.018, 2018

Zhu, C., Chen, T.,and Zhao, L.: Magnesium partitioning into vaterite and its potential role as aprecursor phase in foraminiferal Mg/Ca thermometer. Earth and Planetary Science Letters, 567, 116989, https://doi.org/10.1016/j.epsl.2021.116989, 2021.